Proceedings of the 7th GACM Colloquium on Computational Mechanics
for Young Scientists from Academia and Industry
October 11-13, 2017 in Stuttgart, Germany

High-order accurate time integration methods for electromagnetic-thermal analysis

Tobias Gleim[1]*

Micro Abstract
The inductive heating of a metal shaft is influenced by an alternating current inducing a high frequency electromagnetic field, which causes a temperature increase due to the resulting eddy currents. To examine this process, the fully coupled electromagnetic Maxwell equations are combined with heat conduction. Due to the high frequencies of the applied current and the strongly temperature dependent material parameters, high-order accurate numerical methods in space and time are investigated.

[1]Center for Aerospace Structures, University of Colorado at Boulder, Boulder, United States
***Corresponding author**: tobias.gleim@colorado.edu

1 Introduction

In order to achieve application-optimized material properties, new material composites or novel fabrication sequences are developed. Thus, in the area of metal-forming processes, heating and cooling strategies that locally influence workpiece characteristics such as ductility, hardness, yield strength or impact resistance, are important concepts. The tailor-made combination of properties has been realized in the past by a variety of different materials or extensive manufacturing processes. For components made with just one metal, precisely defined properties can be obtained in the following three stages, see Figure 1. In this integrated manufacturing process, a metal

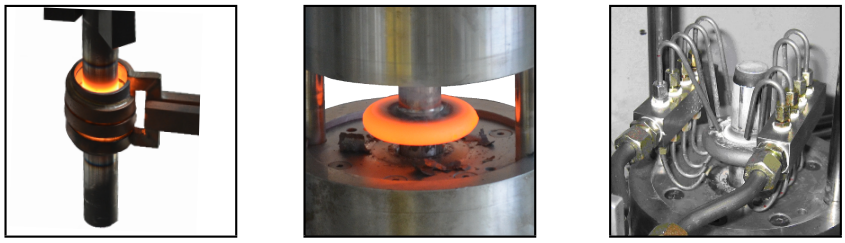

Figure 1. Integrated thermomechanical forming process, cf. [9].

shaft obtains a heterogenous temperature distribution throughout a local inductive heating. Then the heated metal shaft is formed in a press and simultaneously cooled due to the contact with the die. Finally, the desired material properties are achieved by partial rapid cooling, allowing the creation of graded materials with defined properties, cf. [9].

Furthermore the inductive heating process is examined to describe the temperature evolution due to electromagnetical effects. The inductive heating of the shaft is influenced by an alternating current inducing a high frequency electromagnetic field, which causes a temperature increase due to the resulting eddy currents.
To analyze this process, the coupling between the electric and the magnetic field is described by the fully coupled Maxwell equations [4,8]. Moreover the heat conduction equation is considered to describe thermal effects. Since all material parameters are subjected to large changes due to heating, the Maxwell equations and the heat conduction equation are strongly coupled.
In order to solve this coupled electromagnetic-thermo multifield problem the nonlinear heat equation and the electromagnetic equations are formulated in a monolithic approach. In a further

step an axisymmetric case is considered, motivated by the fact that the inductive heating process of a cylindrical shaft is analysed [1,2]. Since the problem is strongly time dependent a high order accurate p-finite element method is applied. The resulting equations are spatially discretized by the standard finite element method [10]. In analogy, the time integration is achieved with high order RUNGE-KUTTA methods [3,5,6].

2 Inductive Heating

The inductive heating process is characterized by the MAXWELL equations and the heat conduction equation, taking into account nonlinear material effects due to temperature changes. In the end this leads to a combination of the weak forms of electric, magnetic and thermal fields, yielding a monolithic system of equations:

$$
\begin{aligned}
\delta W^E &= \int_\Omega \delta\boldsymbol{E}\cdot\epsilon\,\ddot{\boldsymbol{E}}\;dV + \int_\Omega \delta\boldsymbol{E}\cdot\sigma_c(\Theta)\,\dot{\boldsymbol{E}}\;dV + \int_\Omega \delta\boldsymbol{E}\cdot\dot{\sigma}_c(\Theta)\,\boldsymbol{E}\,dV + \int_\Omega \delta\boldsymbol{E}\cdot\dot{\kappa}(\Theta)\,\nabla\times\boldsymbol{B}\,dV \\
&\quad + \int_\Omega \kappa(\Theta)\,\nabla\times\delta\boldsymbol{E}\cdot\nabla\times\boldsymbol{E}\,dV + \int_\Omega \nabla\kappa(\Theta)\times\delta\boldsymbol{E}\cdot\nabla\times\boldsymbol{E}\,dV + \int_\Omega \delta\boldsymbol{E}\cdot\nabla\dot{\kappa}(\Theta)\times\boldsymbol{B}\,dV \\
&\quad + \int_\Omega \delta\boldsymbol{E}\cdot\dot{\boldsymbol{J}}_i\,dV + \int_\Omega \nabla\cdot\boldsymbol{E}\,\kappa(\Theta)\,\nabla\cdot\boldsymbol{E}\,dV - \int_\Omega \nabla\cdot\boldsymbol{E}\,\tfrac{\rho_R}{\epsilon}\,dV = 0 \\
\delta W^B &= \int_\Omega \delta\boldsymbol{B}\cdot\epsilon\,\ddot{\boldsymbol{B}}\;dV + \int_\Omega \nabla\times\delta\boldsymbol{B}\cdot\kappa(\Theta)\,\nabla\times\boldsymbol{B}\,dV + \int_\Omega \nabla\times\delta\boldsymbol{B}\cdot\nabla\kappa(\Theta)\times\boldsymbol{B}\,dV \\
&\quad - \int_\Omega \delta\boldsymbol{B}\cdot\nabla\times\sigma_c(\Theta)\boldsymbol{E}\,dV + \int_\Omega \nabla\cdot\delta\boldsymbol{B}\,\kappa(\Theta)\,\nabla\cdot\boldsymbol{B}\,dV - \int_\Omega \nabla\times\delta\boldsymbol{B}\,\boldsymbol{J}_i\,dV = 0. \\
\delta W^\Theta &= \int_\Omega \delta\Theta\,\rho\,c_p(\Theta)\,\dot{\Theta}\,dV - \int_\Omega \nabla\delta\Theta\cdot\boldsymbol{q}(\Theta)\,dV - \int_\Omega \delta\Theta\,Q\,dV \\
&\quad + \int_{\Gamma_q} \delta\Theta\left[q^\star + \alpha\left[\Theta-\Theta_\infty\right] + \varepsilon_\Theta(\Theta)\,\sigma_\Theta\,A\,\left[\Theta^4-\Theta_\infty^4\right]\right]dA = 0.
\end{aligned}
\tag{1}
$$

Therein, the vectors $\boldsymbol{E}$, $\dot{\boldsymbol{E}}$ and $\ddot{\boldsymbol{E}}$ represent the electric field and their first and second time derivative, the vectors $\boldsymbol{B}$ and $\ddot{\boldsymbol{B}}$ the magnetic field and the second time derivative and the thermal field Θ with the first time derivative $\dot{\Theta}$. The material parameters and further variables are the electric permittivity ϵ, the electric conductivity σ_c, the magnetic permeability μ with $\kappa = 1/\mu$, the electric charge ρ_R, the density ρ, the heat capacity c_p, the heat flux vector $\boldsymbol{q}$ with FOURIER's law $\boldsymbol{q} = -\lambda_\Theta\nabla\Theta$, the thermal conductivity λ_Θ, thermal source term $Q = \boldsymbol{J}_i^2/\sigma(\Theta)$, the external flux vector $q^\star$, the heat transfer coefficient α, the bulk temperature Θ_∞, the emissivity ε_Θ and the STEFAN-BOLTZMANN constant σ_Θ.

2.1 Thermal Material Characterization

Within the first step of the chain process of Figure 1 the steel is heated from room temperature to about 1200K. Due to this large temperature range, the material properties change drastically. To obtain the material properties as a function of the temperature, experimental tests were performed at the Austrian foundry research institute (ÖGI). The resultant data is exploited to generate phenomenological material models for the thermal conductivity $\lambda_\Theta(\Theta)$, the heat capacity $c_p(\Theta)$, the emissivity $\varepsilon_\Theta(\Theta)$, the electric conductivity $\sigma(\Theta)$ and the magnetic permeability $\mu(\Theta)$, cf. [5].

3 Spatial Discretization

To solve the inductive heating process, the next step is to discretize the weak forms (1) of the electric, magnetic and thermal field spatially by using the finite element method. Standard LAGRANGE shape functions are used which allow a general formulation with an arbitrary polynomial degree p in each direction, cf. [5,10]. This nonlinear problem, due to the temperature dependent material properties, is solved via a NEWTON-RAPHSON scheme. Hence, appropriate linearizations have to be performed and evaluated. Thereby, the integration is carried out using

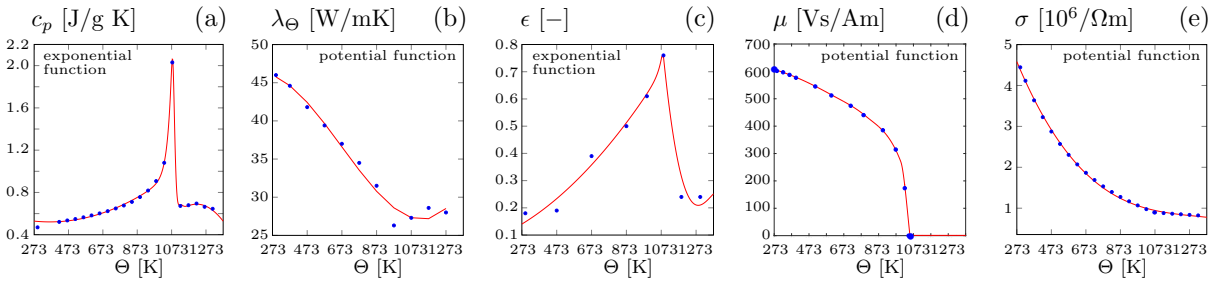

Figure 2. Temperature-dependent material parameters: a) specific heat capacity, b) thermal conductivity, c) emissivity, d) magnetic permeability and e) electric conductivity. Points are experimental data and lines are the courses of the associated phenomenological material models.

the GAUSS-LEGENDRE quadrature. Finally, a general semi-discrete system of linear equations is obtained:

$$\mathbf{M}_t \cdot \Delta\ddot{\mathbf{u}} + \mathbf{D}_t \cdot \Delta\dot{\mathbf{u}} + \mathbf{K}_t \cdot \Delta\mathbf{u} = \mathbf{r} - \mathbf{r}_{int}. \tag{2}$$

The matrices $\mathbf{M}_t$, $\mathbf{D}_t$ as well as $\mathbf{K}_t$ are the linearizations of the weak forms, here denoted as inner $\mathbf{r}_{int}$ and outer $\mathbf{r}$ flux vector, with respect to the second, first and zeroth order time derivative of the primary variable vector $\mathbf{u}$. Therein, the vector $\mathbf{u} = [\mathbf{E}, \mathbf{B}, \Theta]^T$ of primary variables for the inductive heating process is introduced together with its time derivatives to obtain an abridged form. The variable $\Delta\mathbf{u}$ and its time derivatives are the increments of the primary variable $\mathbf{u}$ and its time derivatives, obtained through the linearization with proper GÂTEAUX derivatives.

4 Temporal Discretization

In order to be able to solve the ordinary system of equations (3), a temporal discretization has to be carried out. Therefore, classical stiffly accurate diagonal implicit RUNGE-KUTTA schemes will be applied, cf. [3,7]. In this type of RUNGE-KUTTA methods, the primary variables and the increments are solved at the points in time $t_{ni} = t_n + \Delta t\ c_i$, the so-called stages s. The approximation of the variables and increments is done using special quadrature rules and weighting factors a_{ij}, cf. [3,6]. Since for the studies in this paper stiffly accurate diagonal RUNGE-KUTTA methods are used and thereby the last stage $t_{ns} = t_{n+1}$ is the solution at the end of the time step, the external integration with the b_j-factors is not required. By evaluating the semi-discrete balance equation with the RUNGE-KUTTA approximations, equation (3) can be reformulated as follows:

$$\left[\mathbf{M}_t \frac{1}{[\Delta t\ a_{ii}]^2} + \mathbf{D}_t \frac{1}{[\Delta t\ a_{ii}]} + \mathbf{K}_t\right] \Delta\mathbf{u}_{ni} = \mathbf{r} - \mathbf{r}_{int}. \tag{3}$$

The parameters c_i, a_{ij} and b_j can be determined using BUTCHER-tableaus, cf. [3,6].

5 Simulation of a Steel Shaft

As a numerical example for the above deduced theory, the inductive heating process of a 51CRV4 shaft will be examined in an axisymmetric case, see Figure 3. The present example is used to study the h-error and the embedded error for the stiffly accurate diagonal RUNGE-KUTTA methods with respect to the accuracy. Three different BUTCHER-tableaus with different time step sizes are investigated, cf. [5]. If the error curves, see Figure 4 left, of all methods are summarized for each time step size, it is possible to determine the corresponding order of convergence, see Figure 4 right. The example obtains for the implicit EULER method a global order of convergence of the h-error of $\mathcal{O} \approx \Delta t^1$, see Figure 4. The two- and three-stage stiffly accurate diagonal RUNGE-KUTTA method lead to a higher global order of $\mathcal{O} \approx \Delta t^2$ and $\mathcal{O} \approx \Delta t^3$, respectively. The order of accuracy of the embedded error of the two- and three-stage method is as stated in the literature an order less than the order of accuracy of the h-error, and that is what is demonstrated in Figure 4 right, cf. [3,6].

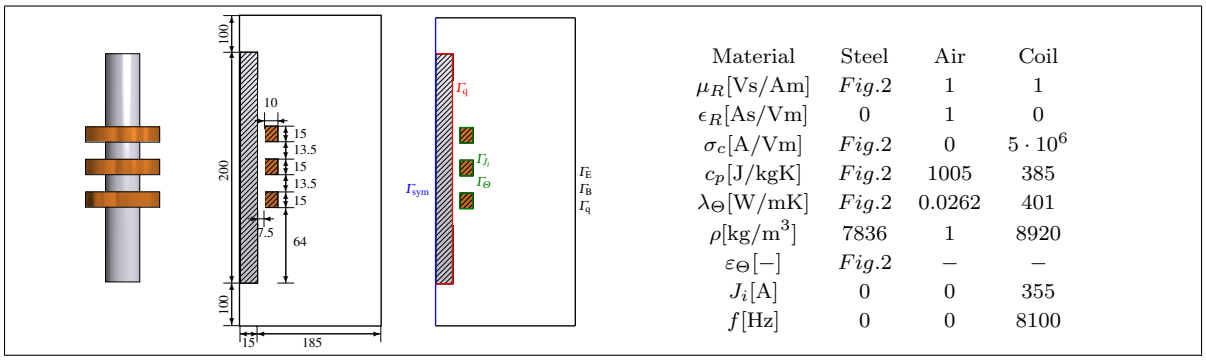

Material	Steel	Air	Coil
μ_R[Vs/Am]	*Fig.*2	1	1
ϵ_R[As/Vm]	0	1	0
σ_c[A/Vm]	*Fig.*2	0	$5 \cdot 10^6$
c_p[J/kgK]	*Fig.*2	1005	385
λ_Θ[W/mK]	*Fig.*2	0.0262	401
ρ[kg/m^3]	7836	1	8920
ε_Θ[−]	*Fig.*2	–	–
J_i[A]	0	0	355
f[Hz]	0	0	8100

Figure 3. Axisymmetric depiction of the steel shaft for the inductive heating process with dimensions (left), boundary conditions (middle) and the material parameters and load (right).

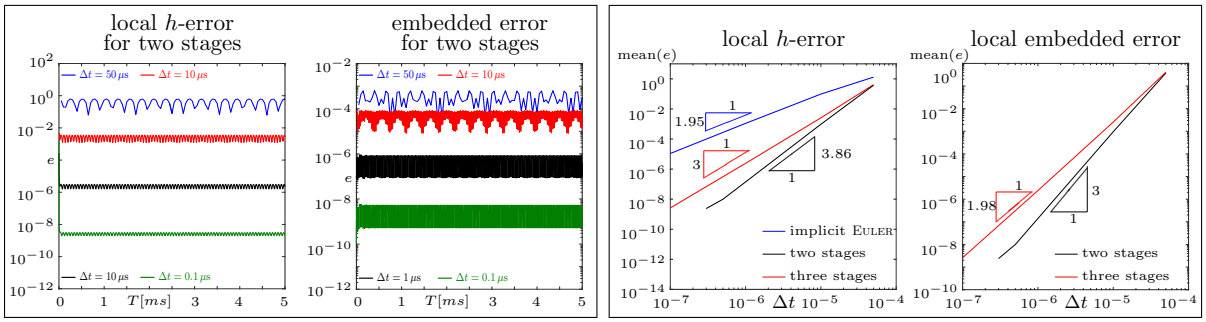

Figure 4. Plot of the error curves for a two stage Runge-Kutta scheme (left) and order of accuracy (right) for the local h-error and local embedded error for different Runge-Kutta schemes.

References

[1] F. Assous, P. Ciarlet, S. Labrunie, and J. Segré. Numerical solution to the time-dependent Maxwell equations in axisymmetric singular domains: The singular complement method. *Journal of Computational Physics*, 191:147–176, 2003.

[2] R. Beck, P. Deuflhard, R. Hiptmair, R. Hopper, and B. Wohlmuth. Adaptive multilevel methods for edge element discretizations of Maxwell's equations. *Surveys of Mathematics for Industry*, 8, 1995.

[3] J. C. Butcher. On runge-kutta processes of high order. *Journal of the Australian Mathematical Society*, 4:179–194, 5 1964.

[4] L. Demkowicz. *Computing with hp-Adaptive Finite Elements: Volume 1: One and Two Dimensional Elliptic and Maxwell Problems.* Chapman & Hall/CRC Applied Mathematics and Nonlinear Science Series, 2006.

[5] T. Gleim. Simulation of Manufacturing Sequences of Functionally Graded Structures. PhD Thesis, 2016.

[6] E. Hairer and G. Wanner. *Solving Ordinary Differential Equations II: Stiff and Differential-Algebraic Problems.* 14. Springer Berlin Heidelberg, 2010.

[7] T. Hughes and G. Hulbert. Space-time finite element methods for elastodynamics: Formulations and error estimates. *Computer Methods in Applied Mechanics and Engineering*, 1(66):339–363, 1988.

[8] V. Rudnev, D. Loveless, R. Cook, and M. Black. *Handbook of Induction Heating.* Marcel Dekker, Inc., 2003.

[9] K. Steinhoff, U. Weidig, and N. Saba. Investigation of plastic forming under the influence of locally and temporally variable temperature and stress states. In K. Steinhoff, H. Maier, and D. Biermann, editors, *Functionally Graded Materials in Industrial Mass Production*, pages 35–52. Verlag Wissenschaftliche Scripten, Auerbach, 2009.

[10] O. Zienkiewicz and R. Taylor. *The Finite Element Method.* Butterworth Heinemann, 2000.